The Shape of a Fluid Drop Trapped Between Two Horizontal Surfaces

In a close packed dispersion, a drop experiences forces from the surrounding drops which affect its shape and rate of coalescence. The geometry is complicated, but a simple model which may help clarify the phenomenon is that of a drop trapped between two horizontal surfaces under the action of an applied force.

The differential equations governing the shape of the surface of such a drop have been solved numerically and the predicted drop dimensions checked experimentally by applying known forces to a drop and recording the shape photographically.

S. M. WOOD

Shell Chemicals (U.K.) Ltd.
Stanlow Refinery, England

S. HARTLAND

Swiss Federal Institute of Technology
Zurich, Switzerland

SCOPE

The rate of approach of a drop to another drop, a fluid-liquid interface, or solid surface is determined by the rate of drainage of the intervening fluid film. When the film becomes sufficiently thin at some point, it ruptures and the drop coalesces with its homophase or wets the surface.

The rate of drainage decreases as the area of the film increases and as the force pressing the surfaces of the film together increases. For the gravitational approach of a single drop the applied force depends on the drop volume and the density difference with the surrounding fluid. The area of the draining film also depends on these properties and in addition on the interfacial tension. For a single drop approaching a horizontal plane (Hartland, 1967a, 1969a) and a deformable fluid-liquid interface (Hartland 1967b, 1967c, 1968), the area does not change with time (Hartland 1969b) and may be calculated (Bashforth and Adams, 1883; Princen, 1963).

However no information is available when an additional force is applied to the drop such as may arise from the presence of surrounding drops in close packed dispersions. A drop at the coalescing interface experiences a vertical force due to the drops above it and a horizontal force due to the other drops at the interface. The vertical force tends to increase the area of the draining film between the drop and the bulk interface and the horizontal force to decrease this area. The vertical force is the weight of the drops less their buoyancy force plus the viscous drag acting on them because they are approaching the coalescing interface. A drop in the bulk of the dispersion experiences similar forces from the surrounding drops. Drops are also pressed against the wall of the vessel containing the dispersion and other internal surfaces.

This paper considers the effect of a vertical force on the shape of a drop trapped between two horizontal planes when the drop is separated from each plane by a draining film. The problem has intrinsic interest for the wetting of solid surfaces and provides a possible model for the coalescence of a drop with another drop, or a bulk fluid-liquid interface within a close packed fluid-liquid dispersion. In this respect, however, it does not allow for the constraining effect of the horizontal forces from surrounding drops. When high concentrations of surface active agent are present, the area of the draining film may change with time under certain circumstances as found by Hodgson and Woods (1969). This is also true for collisions between two drops which possess considerable momentum and may be oscillating before impact, as found by Scheele and Lang (1971). However, for relatively pure systems in which only gravitational forces are present, the drop dimensions and in particular the areas of the draining films will remain constant as assumed in this paper.

CONCLUSIONS AND SIGNIFICANCE

The differential equations governing the shape of the free fluid-liquid interface of a drop trapped between two horizontal surfaces are derived and integrated numerically so that the areas of the draining films and other characteristic drop dimensions may be tabulated in terms of the applied force, drop volume, and physical properties.

This information provides a basis for assessing the effect of applied force on the rates of drainage of the films above and below the drop. An indication of whether to expect interdroplet coalescence in a close packed fluid-liquid dispersion may thus be obtained.

As a check on the theoretical results, the dimensions are also obtained experimentally by applying known forces to a drop and recording its shape photographically. The experimental dimensions agree with those theoretically predicted to better than 5%, which is within the limits of experimental error.

Correspondence concerning this paper should be addressed to S. Hartland.

THEORY

Consider the drop of volume v_d and density ρ_h immersed in a lighter fluid of density ρ_l and trapped between two horizontal planes as shown in Figure 1. In addition to the force due to the hydrostatic pressure, there are forces f_t and f_b acting on the upper and lower planes respectively such that the difference between them is equal to the weight of the drop less its buoyancy force. The drop is symmetrical about its vertical axis; at any point in the surface of the drop the radial distance from the axis is x, the vertical distance from the top of the drop is y and the volume of the drop between the top plane and the horizontal plane at y is v. The length of the free drop surface is s and its inclination to the upper plane measured through the ambient fluid is Φ. There are draining films between the drop and each of the planes, so that Φ varies between 0 and π. The radius of the periphery of the upper draining film is x_t and of the lower film is x_b. The average dynamic pressure in the top film (measured relative to the hydrostatic pressure) is $f_t/\pi x_t^2$. In the absence of circulation, this is also the excess pressure inside the top of the drop above that in the ambient fluid because the net vertical force due to the excess pressure in the draining film above that in the drop is zero (Hartland 1969), even though the film may be nonuniform in thickness. Equating the excess pressure in the drop above that in the ambient fluid to the stress in the drop surface at any point thus gives

$$\frac{f_t}{\pi x_t^2} = \sigma\frac{d\Phi}{ds} + \sigma\frac{\sin\Phi}{x} - \Delta\rho g y \qquad (1)$$

where σ is the interfacial tension and $\Delta\rho = \rho_h - \rho_l$.

In order to reduce the number of variables, it is convenient to define the dimensionless quantities

$$S = sc^{1/2}; \quad X = xc^{1/2}; \quad Y = yc^{1/2} \qquad (2)$$

$$V = vc^{3/2}; \quad F = fc^{1/2}/\sigma \qquad (3)$$

where $c = \Delta\rho g/\sigma$. Equation (1) may thus be rewritten

$$\frac{d\Phi}{dS} = \frac{F_t}{\pi X_t^2} + Y - \frac{\sin\Phi}{X} \qquad (4)$$

and in addition we may relate Y, X, and V to S and Φ by the equations

$$\frac{dY}{dS} = \sin\Phi \qquad (5)$$

$$\frac{dX}{dS} = \cos\Phi \qquad (6)$$

$$\frac{dV}{dS} = \pi X^2 \sin\Phi \qquad (7)$$

The boundary conditions at the upper plane are

$$\Phi = 0; \quad S = 0; \quad Y = 0; \quad X = X_t; \quad V = 0 \qquad (8)$$

and at the lower plane

$$\Phi = \pi; \quad S = S_b; \quad Y = Y_b; \quad X = X_b; \quad V = V_d \qquad (9)$$

The downward force acting on the volume v is $f_t + v\rho_h g + 2\pi\chi\sigma\sin\Phi$ plus the force due to the hydrostatic pressure in the ambient fluid acting on the upper plate and the free drop surface. The sum of these forces is balanced by the force due to the pressure inside the drop acting upwards on the horizontal plane at y. This pressure is equal to the local value of the hydrostatic pressure in the ambient fluid plus the excess pressure inside the drop. The net effect of the hydrostatic pressure acting on the complete surface surrounding the volume v is the buoyancy force $v\rho_l g$ by Archimedes principle and the force due to the excess pressure acting on the horizontal plane at y is $\pi x^2(f_t/\pi x_t^2 + \Delta\rho g y)$. A force balance on the volume v thus leads to

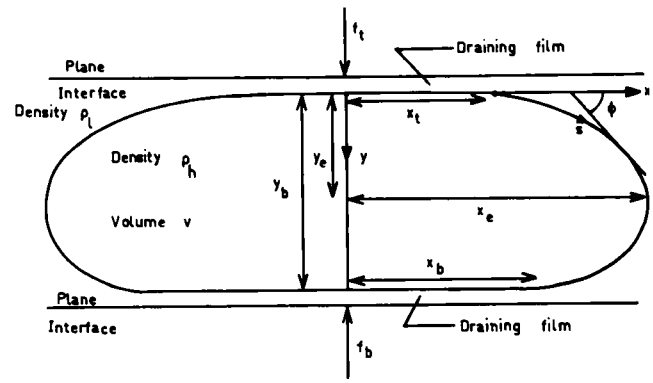

Fig. 1. Dimensions of a drop trapped between two horizontal surfaces.

$$F_t + V + 2\pi X\sin\Phi = \pi X^2\,(F_t/\pi X_t^2 + Y) \qquad (10)$$

At the surface of the lower plane $\Phi = \pi$, $Y = Y_b$ and the excess pressure inside the drop is $F_b/\pi X_b^2$, so the force balance on the whole drop is

$$F_t + V_d = F_b \qquad (11)$$

For given values of F_t and X_t, increments $d\Phi$, dY, dX, and dV may be calculated for a given increment dS, from Equations (4) through (7). These enable new values of Φ, Y, X, and V to be obtained from which further increments may be calculated. The starting values of Φ, Y, and X are given by Equation (8). The calculation ceases when $\Phi = \pi$, as indicated by Equation (9). Equation (10) relates the values of F_t, X_t, Φ, Y, X and V and provides a check on the accuracy of the integration. Equation (11) enables the force F_b acting on the bottom plate to be calculated once the drop volume at $\Phi = \pi$ has been obtained.

The arc length S may be eliminated from Equations (4) through (7) which become

$$\frac{dY}{d\Phi} = \frac{\sin\Phi}{F_t/\pi X_t^2 + Y - \dfrac{\sin\Phi}{X}} \qquad (12)$$

$$\frac{dX}{d\Phi} = \frac{\cos\Phi}{F_t/\pi X_t^2 + Y - \dfrac{\sin\Phi}{X}} \qquad (13)$$

$$\frac{dV}{d\Phi} = \frac{\pi X^2\sin\Phi}{F_t/\pi X_t^2 + Y - \dfrac{\sin\Phi}{X}} \qquad (14)$$

Writing the equations in this form enables the variation in X, Y, and V to be obtained for given increments in Φ.

When the density of the drop is less than that of the ambient fluid, exactly the same equations apply if F_t, X_t, F_b, and X_b are replaced by F_b, X_b, F_t, and X_t respectively and Y is measured upwards from the surface of the bottom plate. The value of c is still positive for ρ_h and ρ_l are replaced by $-\rho_l$ and $-\rho_h$ respectively, so that $\Delta\rho$ is unchanged.

When there is no force acting on the top of the drop, both F_t and X_t are zero. The sessile drop then sits on the bottom plate under the action of its own weight less the

buoyancy force and the excess pressure in the top of the drop, where the radius of curvature is b, is equal to $2\sigma/b$. Writing $B = bc^{1/2}$ the dimensionless Equations (5) to (7) and (9) are unchanged and Equations (4), (8), (10), and (11) become

$$\frac{d\Phi}{dS} = \frac{2}{B} + Y - \frac{\sin\Phi}{X} \tag{14}$$

$$\Phi = 0; \quad S = 0; \quad Y = 0; \quad X = 0; \quad V = 0; \tag{15}$$

$$V + 2\pi X \sin\Phi = \pi X^2 (2/B + Y) \tag{16}$$

$$V_d = F_b \tag{17}$$

The solution to this set of equations has already been obtained by Bashforth and Adams (1883) and Staicopolus (1962).

SOLUTION OF THE EQUATIONS

A Runge-Kutta technique (Milne, 1953) was used to integrate the differential equations for given values of F_t and X_t. Four substitutions into the equations are required at each step so that for rapid computation it is desirable to use as large an increment as possible. Reducing the increment by trial and error to meet a given accuracy wastes computation time and so it is also desirable that the increment should not vary much throughout the integration. Examination of Equation (13) shows that the initial value of $dX/d\Phi$ is $\pi X_t^2/F_t$ (because the initial values of Y and Φ are initially zero) so that $dX/d\Phi$ is large when X_t is large and F_t is small. Consequently the increment in Φ must be very small to accurately predict the change in X. However, under these conditions $d\Phi/dS$ in Equation (4) is small, so that the increment in S may be large and still accurately predict the change in Φ. Conversely when X_t is small and F_t is large, the initial value of $d\Phi/dS$ is large whereas that of $dX/d\Phi$ is small so that the increment in Φ may be relatively large. Two procedures were therefore employed; one with Φ and the other with S as the independent variable. In the region where the calculation required a very small step length in Φ, S was used as the independent variable and vice versa. In practice S was used as the independent variable when $d\Phi/dS < 1$ and Φ as the independent variable when $d\Phi/dS > 1$. In this way, it is possible throughout the calculation to use a relatively large step length to which only small modifications have to be made to keep the error within a predetermined value. The values of X and Y at $\Phi = \pi/2$ were obtained without interpolation by returning to the previous step as soon as the angle Φ passed this value and then using Φ as the independent variable advancing an increment $d\Phi$ which made Φ exactly $\pi/2$. The calculation was then allowed to proceed in the manner described above until Φ passed π when by a similar procedure X, Y, and V were obtained at exactly $\Phi = \pi$.

The accuracy of the Runge-Kutta method is not easy to estimate, but the error is of the fifth order in the step length for each step. Fortunately, it is possible to make an independent estimate using the force balance given by Equation (10). This enables the exact volume V to be calculated for given values of X, Y, and Φ, and hence the exact change in volume for a given increment in Φ may be obtained from the difference between the two values of V at the beginning and end of the increment. If this increment in V differed from that calculated using Equation (7) by more than 1%, the step size was reduced and the calculation repeated. Initially the step length was 1° for Φ and 0.01 for S, but these fell in some instances to 10^{-2} and 10^{-4} respectively. The large step lengths were however particularly useful in the region of $\Phi = \pi/2$, where a high degree of accuracy is easy to achieve. The integrated volume V may also be compared with that obtained from a force balance; the accuracy of the agreement gradually increased with Φ and at $\Phi = \pi$ the two values always agreed to better than 10^{-2}%.

THEORETICAL RESULTS AND DISCUSSION

Values of the dimensionless variables X_e, Y_e, X_b, Y_b, and V were calculated for different dimensionless forces F_t ranging between 0.001 and 10,000 and different values of X_t chosen such that the calculated value of V is between 0.01 and 1000. Figures 2 to 6 show the variation in X_t, X_e, Y_e, X_b, and Y_b with V for different values of F_t. These figures show that for a constant drop volume as F_t in-

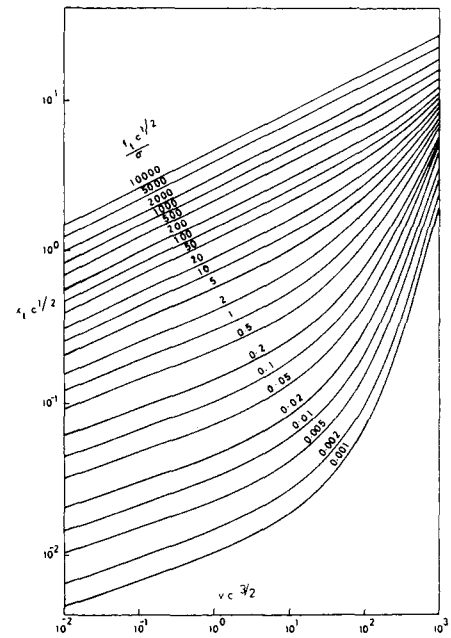

Fig. 2. Variation of $x_t c^{1/2}$ with $Vc^{3/2}$ for different values of $f_t c^{1/2}/\sigma$.

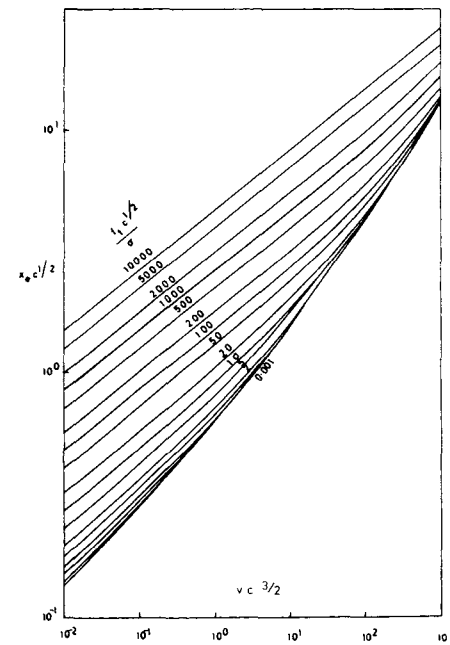

Fig. 3. Variation of $x_e c^{1/2}$ with $Vc^{3/2}$ for different values of $f_t c^{1/2}/\sigma$.

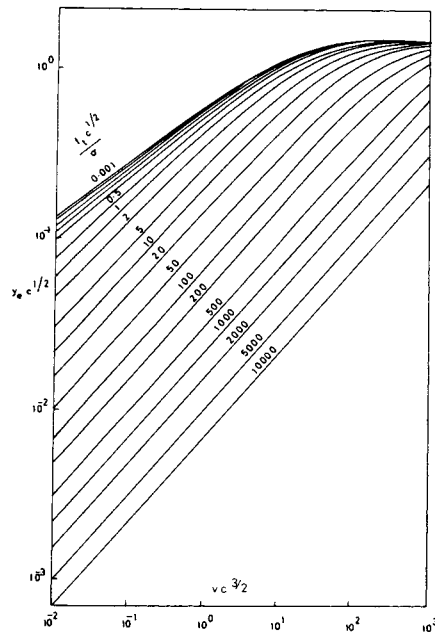

Fig. 4. Variation of $y_e c^{1/2}$ with $vc^{3/2}$ for different values of $f_t c^{1/2}/\sigma$.

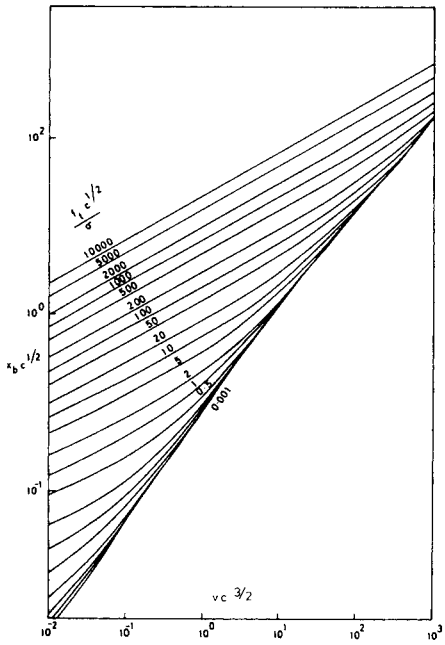

Fig. 5. Variation of $v_b c^{1/2}$ with $vc^{3/2}$ for different values of $f_t c^{1/2}/\sigma$.

creases the values of Y_e and Y_b decrease and X_t, X_e, and X_b increase; as expected, the drop becomes more and more flattened by the applied force. As F_t approaches zero, the values of X_e, Y_e, X_b, and Y_b converge to the values predicted for a sessile drop with no applied force by the tables of Bashforth and Adams (1883). When $F_t = 0.001$, the agreement is better than 1% for small drop volumes and becomes almost exact at large drop volumes. This is a severe test of the accuracy of the integration because $F_t/\pi X_t^2$ is replaced by $2/B$ in the equation for a sessile drop and so must remain finite as F_t approaches zero.

It is important to examine the effect of the applied force on the areas of the top and bottom draining films as these affect the rate of drainage. Figures 7 and 8 show that as the applied force is increased for a drop of constant volume, the areas of both films increase. The effect of the applied force and drop volume on the ratio of the areas is shown in Figure 9. The area of the top film is always less than the area of the bottom film, but the ratio rapidly approaches 1 for large forces. As the drop volume increases, the ratio passes through a minimum which becomes more pronounced as the applied force decreases. Very small sessile drops are almost spherical and a small force flattens the top of such a drop almost as much as the bottom. On the other hand, large sessile drops are already flattened due to their own weight and so the area of the upper draining film again approaches that of the lower film when a force is applied. For drops of intermediate size, however, the greater force pressing on the bottom film causes its area to be correspondingly greater

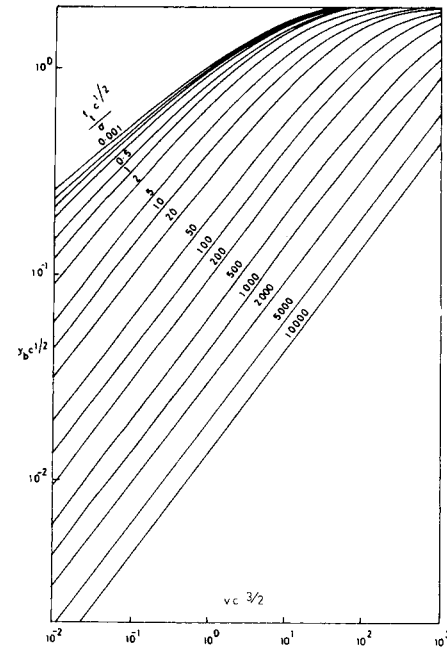

Fig. 6. Variation of $y_b c^{1/2}$ with $vc^{3/2}$ for different values of $f_t c^{1/2}/\sigma$.

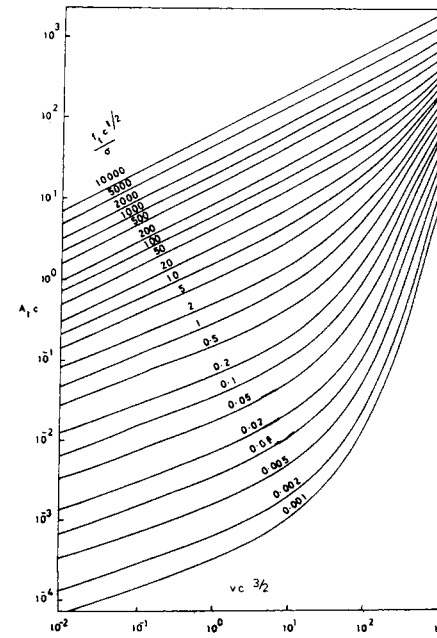

Fig. 7. Variation of $A_t c$ with $vc^{3/2}$ for different values of $f_t c^{1/2}/\sigma$.

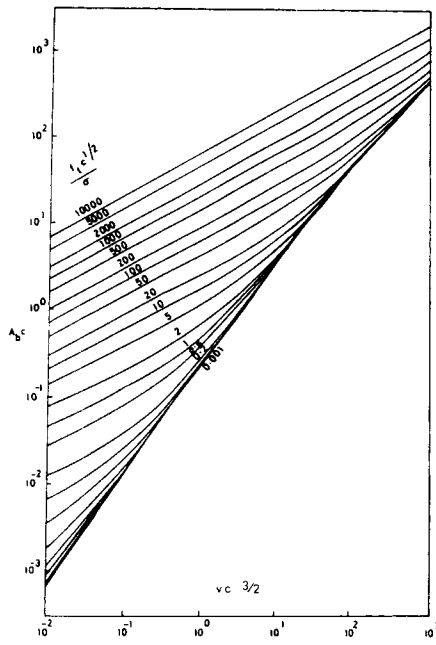

Fig. 8. Variation of $A_b c$ with $vc^{3/2}$ for different values of $f_t c^{1/2}/\sigma$.

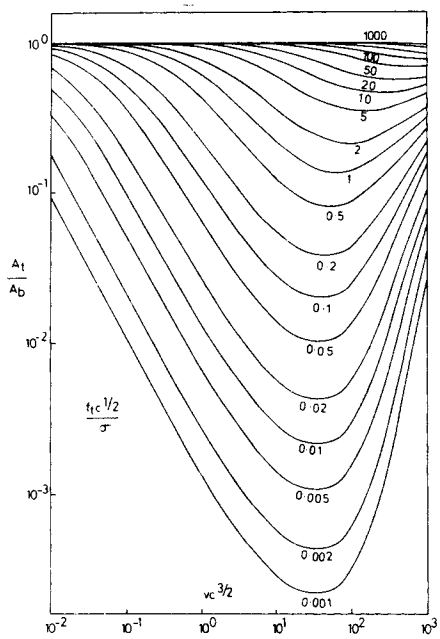

Fig. 9. Variation of A_t/A_b with $vc^{3/2}$ for different values of $f_t c^{1/2}/\sigma$.

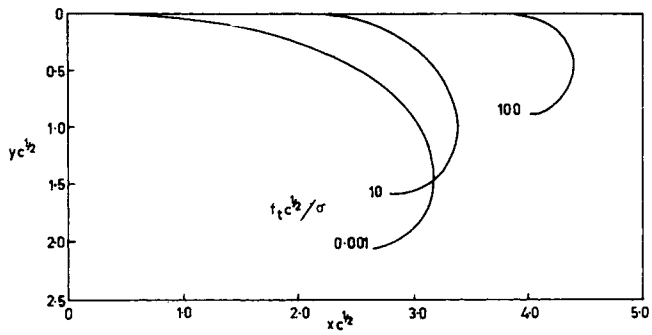

Fig. 10. Profiles of a drop of dimensionless volume $vc^{3/2} = 50$ calculated for three different applied forces $f_t c^{1/2}/\sigma = 0.001$, 10, and 100.

TABLE 1. PHYSICAL PROPERTIES OF THE LIQUIDS USED AT 22.5°C

Physical property	50% v/v sextol phthalate-liquid paraffin	Golden syrup + 10% v/v satd. aq. *KI*	Silicone fluid MS 200	41.5% v/v aqueous golden syrup ½% v/v satd. aq. *KI*
Refractive index	1.495	1.497	1.404	1.405
Density, ρ, g/cm³	0.9770	1.4664	0.97	1.1875
Viscosity, Ns/m^2	0.46	0.72	12.125	0.00592
Interfacial tension, σ, J/m^2	0.02574		0.0378	
$c = \Delta\rho g/\sigma$, cm^{-2}	19.09		5.64	

than that of the top film.

Examination of the values of X_t, X_e, Y_e, X_b, and Y_b in Figures 2 to 6 shows that for large dimensionless forces the free drop surface is approximately spherical especially for small drop volumes. In addition, the ratio A_t/A_b is close to 1 in this region, as noted above. The approximation that the free drop surface is spherical and the areas of the upper and lower films equal (Charles and Mason, 1960) can thus be seen to hold where the applied force is very large and the drop volume is small. However, in general, the drop surface is not spherical as shown in Figure 10 which gives the profiles for a drop of fixed volume under the action of different forces.

EXPERIMENT

Two liquid-liquid systems were employed. In the first, the light liquid was a solution of 50% v/v Howflex Sextol Phthalate in Boots liquid paraffin BP, and the heavy liquid Lyles Golden Syrup (containing 10% by volume of aqueous potassium iodide, saturated at 22.5°C.). In the second system, the light liquid was Silicone Fluid MS 200 manufactured by Midland Silicones Limited and the heavy liquid 41.5% by volume aqueous Golden Syrup (containing ½% by volume aqueous potassium iodide saturated at 22.5°C.). The physical properties of these liquids are presented in Table 1; the addition of potassium iodide solution brought the refractive indices of the light and heavy liquids close together. The refractive indices were measured on an Abbé-refractometer and the interfacial tensions using the pendant drop method (Andreas et al., 1938). The viscosities were determined using an Ostwald U-tube and a Ferranti-Shirley cone and plate viscometer.

All pieces of apparatus that came into contact with the liquids were thoroughly cleaned; the items were washed with detergent and hot water and then given successive rinses with distilled water and acetone. The apparatus was then soaked in 2% Decon 75 before being given a final rinse with distilled water.

The shape of drops trapped between two horizontal plates was measured photographically. Photographs were taken with an Exacta 35 mm camera using a Zeiss Jena 50 mm Pancolor lens (with extension tubes of varying length according to the magnification required). The camera was mounted on an optical bench and carefully leveled together with a flash gun and screen as shown in Figure 11. A stainless steel plate, 4.5 cm. sq. and 0.3 cm. thick was ground and polished on both sides to an accuracy of greater than 10^{-3} cm. and placed in a cubical glass cell with sides 5 cm. long, which was then filled with the light liquid. Two techniques were employed to measure the applied force, as described below.

Top Pan Balance Technique

This method employs a Mettler top-pan balance (accurate to within ± 0.001 gm) to measure the applied force. A dia-

gram of the apparatus is given in Figure 11. The cubical glass cell was placed on the top-pan balance which had been carefully leveled. A ground and polished stainless steel plate 1.5 cm. sq. was attached to a syringe needle which passed through the plate and protruded about 0.015 cm. on the other side. The syringe was firmly mounted on the optical bench. The clamps used being precisely machined so that the syringe needle was vertical. The balance was tared with the top and bottom plates at a predetermined small separation. The pan was depressed to increase the separation and the drop released. As it fell towards the bottom plate, the cell was moved sideways relative to the syringe tip and the pan released, so that drop became trapped between the smooth surfaces of the two plates. The final reading on the balance less the weight of the drop was the force applied to the drop through the top plate.

The error in this measurement introduced by changing the weight of liquid displaced by the syringe needle resulting from the injection of the drop and the final depression of the balance pan was less than one part per thousand for the largest drops investigated. The order of magnitude of the applied force cannot be predetermined before the experiment, but increases as the initial separation of the plates decreases. A different technique was therefore used in some experiments; the drop was introduced from the Hamilton syringe some distance away from the bottom plate and the top plate was lowered and moved sideways by a screw mechanism until it deformed the drop. The vertical distance moved by the syringe needle was measured using a cathetometer. The applied force was then the final balance reading less the weight of the drop plus the weight of the light fluid displaced by the movement of the syringe needle. Both liquid-liquid systems were studied in this manner for a range of drop sizes and applied forces.

Plunger Technique

Light aluminum plungers 7.5 cm. long, with polished bases 2-cm. diam. were used to apply the forces to the top of drops of Golden Syrup containing aqueous potassium iodide. The plungers were hollow, and by changing their weight the applied force could be altered. The shaft of the plunger moved in a tubular support but could be held in position by a small screw in the side of the tube. The drops were formed from a Hamilton gas-tight syringe (accurate to ± 0.002 ml.) and introduced via a syringe needle beneath the base of the plunger when it was in its fixed position. The plunger was released to compress the drop between the stainless steel plate and its base, as shown in Figure 12. The vertical orientation of the plunger shaft was maintained after release by the two supporting rings on the plunger support. The plunger and support were accurately machined, the rings being only 0.08 cm. thick and 0.01 cm. greater in diameter than the plunger shaft. This design minimized the viscous drag on the plunger. The force exerted by the plunger was taken to be its weight less the buoyancy force and was obtained by weighing the plunger in the light liquid.

It was only possible to construct plungers such that the applied force was relatively large and the drop then deforms to such an extent, that the close justaposition of the plunger base and the flat plate makes uniform illumination of the drop

Table 2. Comparison of Some Experimental and Theoretical Dimensions of Drops to Which an External Force is Applied for Two Liquid-Liquid Systems and Two Methods of Measuring the Applied Force

Experimental							Theoretical				
$x_t c^{1/2}$	$x_e c^{1/2}$	$y_e c^{1/2}$	$x_b c^{1/2}$	$y_b c^{1/2}$	$f_t c^{1/2}$	$vc^{3/2}$	$x_t c^{1/2}$	$x_e c^{1/2}$	$y_e c^{1/2}$	$x_b c^{1/2}$	$y_b c^{1/2}$
Aqueous golden syrup drops in silicone fluid—balance technique											
0.28	0.61	0.34	0.34	0.67	1.04	0.67	0.29	0.62	0.36	0.34	0.69
0.37	0.65	0.31	0.38	0.57	2.00	0.67	0.38	0.66	0.30	0.41	0.58
0.36	0.78	0.45	0.45	0.83	1.35	1.34	0.37	0.79	0.45	0.47	0.83
0.55	0.91	0.33	0.63	0.68	3.50	1.34	0.54	0.87	0.35	0.59	0.66
0.22	0.86	0.62	0.44	1.08	0.37	2.01	0.22	0.87	0.65	0.47	1.11
0.65	1.06	0.39	0.73	0.69	4.24	2.01	0.64	1.01	0.39	0.71	0.73
0.59	1.06	0.48	0.71	0.88	2.90	2.68	0.59	0.11	0.50	0.71	0.90
0.73	1.16	0.45	0.82	0.84	4.78	2.68	0.72	1.12	0.42	0.80	0.78
0.36	1.05	0.67	0.63	1.15	0.77	3.35	0.36	1.07	0.70	0.65	1.20
0.63	1.14	0.52	0.79	0.94	2.97	3.35	0.62	1.14	0.53	0.77	0.96
0.38	1.29	0.85	0.80	1.39	0.70	5.36	0.38	1.27	0.83	0.82	0.14
1.32	1.73	0.37	1.37	0.70	16.5	5.36	1.30	1.65	0.36	1.35	0.69
Golden syrup drops in sextol phthalate-liquid paraffin—balance technique											
0.86	1.54	0.66	1.12	1.15	3.95	7.68	0.86	1.56	0.68	1.14	1.17
1.03	1.61	0.59	1.24	1.08	6.34	7.68	1.02	1.63	0.59	1.22	1.05
1.34	1.80	0.45	1.47	0.83	13.7	7.68	1.33	1.79	0.46	1.44	0.85
1.45	1.83	0.41	1.51	0.80	17.3	7.68	1.43	1.85	0.42	1.52	0.76
1.06	1.85	0.76	1.45	1.27	4.86	11.6	1.05	1.84	0.75	1.40	1.26
1.28	1.95	0.64	1.53	1.11	8.64	11.6	1.27	1.94	0.64	1.52	1.11
1.47	2.06	0.56	1.71	0.99	12.6	11.6	1.44	2.02	0.57	1.66	1.01
1.56	2.11	0.52	1.78	0.93	15.2	11.6	1.53	2.07	0.53	1.69	0.95
1.24	2.13	0.83	1.73	1.36	5.69	16.8	1.23	2.14	0.82	1.68	1.36
1.63	2.28	0.64	1.92	1.11	13.3	16.8	1.62	2.30	0.65	1.88	1.13
1.83	2.40	0.56	2.01	1.00	19.2	16.8	1.83	2.41	0.57	2.01	1.01
1.91	2.47	0.51	2.15	0.92	24.2	16.8	1.96	2.50	0.48	2.11	0.86
1.47	2.42	0.89	2.01	1.43	6.89	23.3	1.44	2.44	0.87	1.97	1.41
1.75	2.58	0.75	2.09	1.23	12.0	23.2	1.72	2.54	0.75	2.10	1.26
1.92	2.63	0.67	2.26	1.14	16.3	23.3	1.90	2.63	0.69	2.20	1.17
2.35	2.88	0.51	2.50	0.93	33.6	23.3	2.32	2.91	0.53	2.53	0.94
Golden syrup drops in sextol phthalate-liquid paraffin—plunger technique											
1.60	2.06	0.46	1.71	0.90	16.9	12.5	1.62	2.15	0.53	1.77	0.95
1.74	2.32	0.57	1.92	1.00	16.9	16.7	1.75	2.36	0.60	1.96	1.05
1.87	2.55	0.63	2.12	1.08	16.9	20.8	1.86	2.54	0.65	2.12	1.12
1.76	2.20	0.43	1.82	0.83	22.5	12.5	1.84	2.24	0.63	1.90	0.82
1.93	2.45	0.50	2.02	0.94	22.5	16.7	1.99	2.46	0.50	2.08	0.92
2.07	2.68	0.55	2.26	1.01	22.5	20.8	2.11	2.64	0.55	2.24	1.00

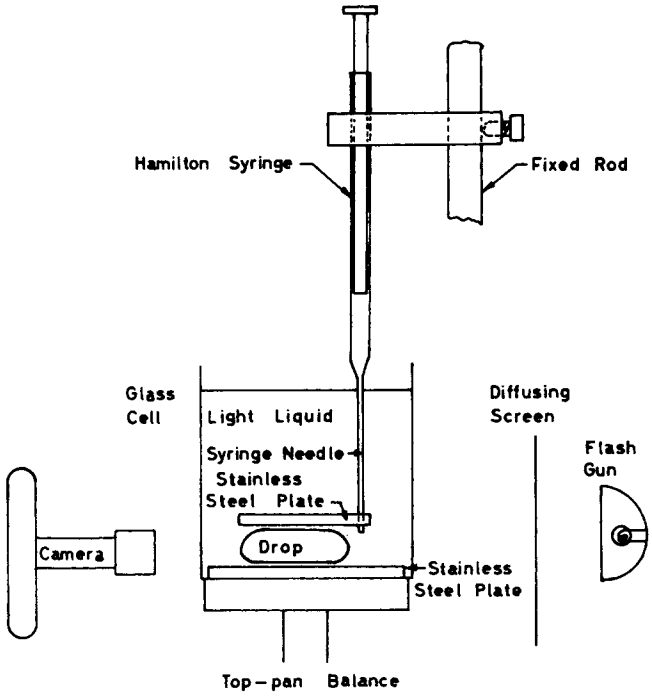

Fig. 11. Experimental arrangement for photography and measurement of force using top-pan balance.

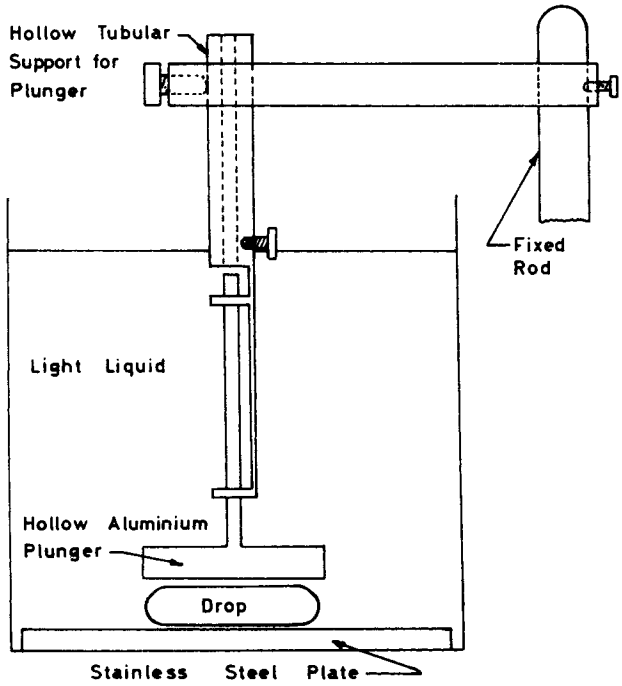

Fig. 12. Experimental arrangement for application of force by means of a plunger.

difficult. On the other hand, only in the case of large applied forces could the viscous drag between the plunger and its support be neglected.

EXPERIMENTAL RESULTS AND DISCUSSION

A typical photograph of a 0.20 ml. drop of golden syrup in 50% v/v sextol phthalate-liquid paraffin trapped between two horizontal plates with a force of $f_t c^{1/2}/\sigma = 5.7$ applied to the upper plate is shown in Figure 13. The negatives were back projected and the magnified drop dimensions measured. The magnification was obtained by comparing the actual diameter of the syringe needle with that of its magnified image. The magnification was usually about 40 times and the magnified dimensions could be read to about 0.05 cm., so that actual dimensions could be measured to 10^{-3} cm., which usually represented an accuracy of better than 1%.

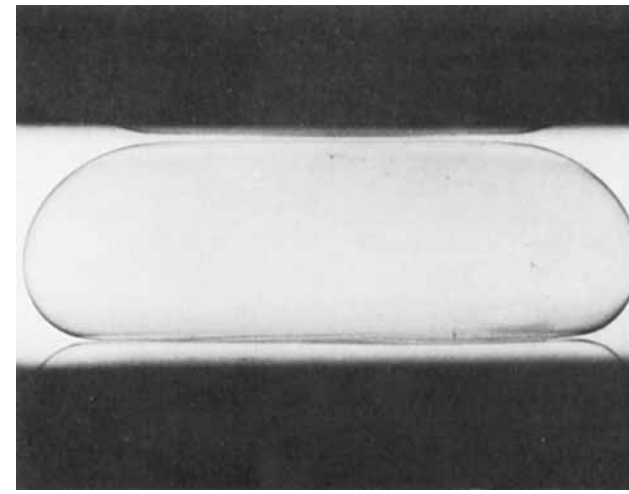

Fig. 13. Photograph of 0.20 ml drop of golden syrup in 50% v/v sextol pthalate-liquid paraffin trapped between two horizontal plates with a force $f_t c^{1/2}/\phi = 5.7$ applied to the upper plate.

The experimental drop dimensions obtained for the two liquid-liquid systems and the two techniques for measuring the applied force and the corresponding theoretical dimensions $x_t c^{1/2}$, $x_e c^{1/2}$, $y_e c^{1/2}$, $x_b c^{1/2}$, $y_b c^{1/2}$ for the same drop volume and applied force are compared in Table 2. The theoretical drop dimensions were obtained by 3-point Lagrange interpolation in the table of numerical values used to plot Figures 2 to 6. The experimental determination of the drop volume and applied force was accurate to ± 1% and this error may be magnified in the predicted drop dimensions. Agreement between the experimental and theoretical drop dimensions is usually to within 5% which is within the limits of the experimental error.

ACKNOWLEDGMENT

The work described in this paper was financed by the Warren Spring Laboratory, Stevenage, England. Mr. R. W. Hartley assisted with the numerical integration of the differential equations.

NOTATION

b = radius of curvature at top of sessile drop
B = dimensionless radius of curvature $bc^{1/2}$
c = constant characterizing physical properties, $(\rho_h - \rho_l)\, g/\sigma$
f = force acting on plate
F = dimensionless force, $fc^{1/2}/\sigma$
g = acceleration due to gravity
s = arc length measured from the upper plate
S = dimensionless arc length, $sc^{1/2}$
v = volume of drop between upper plate and horizontal plane at y
V = dimensionless volume, $vc^{3/2}$
x = radial dimension measured from vertical axis of drop
X = dimensionless distance, $xc^{1/2}$
y = vertical dimension measured from upper plate
Y = dimensionless distance, $yc^{1/2}$

Greek Symbols

Φ = angle of inclination of drop surface to upper plate measured through ambient fluid

ρ = density

Subscripts

b = refers to bottom plate

c = refers to equator of drop

h = refers to heavy fluid

l = refers to light fluid

t = refers to top plate

LITERATURE CITED

Andreas, J. M., E. A. Hauser, and W. B. Tucker, "Boundary Tension by Pendant Drops," *J. Phys. Chem.*, **42**, 1001 (1938).

Bashforth, F., and J. Adams, An Attempt to Test the Theories of Capillary Action, Cambridge Univ. Press, England (1883).

Charles, G. E., and S. G. Mason, "Coalescence of liquid drops with flat liquid-liquid interfaces," *J. Colloid Sci.*, **15**, 236 (1960).

Hartland, S., "The Approach of a Liquid Drop to a Flat Plate," *Chem. Eng. Sci.*, **22**, 1675 (1967a).

———., "The Coalescence of a Liquid Drop at a Liquid-Liquid Interface, I: Drop Shape," *Trans. Inst. Chem. Engrs.*, **45**, T97 (1967b).

———., "The Coalescence of a Liquid Drop at a Liquid-Liquid Interface, II: Film Thickness," *ibid.*, T102 (1967c).

———., "The Coalescence of a Liquid Drop at a Liquid-Liquid Interface, V: The Effect of Surface Active Agent," *ibid.*, **46**, T275 (1968).

———., "The Profile of the Draining Film Beneath a Liquid Drop Approaching a Plane Interface," *Chem. Eng. Progr. Symp. Ser. No. 91*, **65**, 82 (1969a).

———., "The Shape of a Fluid Drop Approaching an Interface," *Can. J. Chem. Eng.*, **47**, 221 (1969b).

Hodgson, T. D., and D. R. Woods, "The effect of surfactants on the coalescence of a drop at an interface. II" *J. Colloid Interface Sci.*, **30**, 429 (1969).

Milne, W. E., Numerical Solution of Differential Equations, Chapman & Hall, London, pp. 72-79 (1953).

Princen, H. M., "Shape of a Fluid Drop at a Liquid-Liquid Interface," *J. Colloid Sci.*, **18**, 178 (1963).

Scheele, G. F., and D. E. Lang, "An Experimental Study of Factors Which Promote Coalescence of Two Colliding Drops Suspended in Water—I," *Chem. Eng. Sci.*, **26**, 1867 (1971).

Staicopolus, D. N., "The Computation of Surface Tension and of Contact Angle by the Sessile Drop method." *J. Colloid Sci.*, **17**, 439 (1962).

Manuscript received February 9, 1972; revision received April 4, 1972; paper accepted April 5, 1972.

Damping Coefficient Design Charts for Sampled-Data Control of Processes with Deadtime

Design charts that give the value of the gain of a proportional sampled-data controller for various closed loop damping coefficient specifications are presented. Charts for first- and second-order processes with various deadtimes are given over a range of sampling rates.

Typical root locus plots in the z plane are also presented to illustrate how increasing deadtime (as an integer multiple of the sampling period) increases the order of the system in the z domain.

W. L. LUYBEN

Department of Chemical Engineering
Lehigh University
Bethlehem, Pennsylvania 18015

SCOPE

The objective of this paper is to provide charts that the control systems designer can use to tune proportional sampled-data controllers.

With the rapidly increasing numbers of chromatographic control loops and digital process control computers, particularly the recent surge is minicomputers, chemical engineers must deal with sampled-data control systems more and more frequently. Straight-forward, easy-to-use charts should help to simplify the design and tuning of these sampled-data loops.

Previous workers have dealt extensively with sampled-data theory and mathematics (Tou, 1959), but applications-oriented papers have been few. The dependence of the maximum stable gain or the so-called "ultimate gain" on deadtime and sampling period has been studied (Mosler et al., 1966) for first-order processes. These authors also present curves for the gain that gives quarter-decay ratio performance. Designers also commonly use other specifications, such as the frequency-domain specifications of gain and phase margins and maximum closed loop log modulus (Luyben, 1971) or the time-domain specification of closed loop damping coefficient. The latter is employed in this paper.

CONCLUSIONS AND SIGNIFICANCE

Simple charts can be easily used to design sampled-data control loops for a desired closed loop damping coefficient specification. Increasing deadtime or sampling rate reduces the allowable gain for a given damping coefficient. However, for a given process with a fixed deadtime, the controller gain may be increased in some cases by decreasing the sampling rate or increasing the sampling period.